

Depth-Aware Action Recognition: Pose-Motion Encoding through Temporal Heatmaps

Mattia Segu, Federico Pirovano, Gianmario Fumagalli, Amedeo Fabris
ETH Zurich

{segum, fpirovan, gfumagal, afabris}@ethz.ch

Abstract

Most state-of-the-art methods for action recognition rely only on 2D spatial features encoding appearance, motion or pose. However, 2D data lacks the depth information, which is crucial for recognizing fine-grained actions. In this paper, we propose a depth-aware volumetric descriptor that encodes pose and motion information in a unified representation for action classification in-the-wild. Our framework is robust to many challenges inherent to action recognition, e.g. variation in viewpoint, scene, clothing and body shape. The key component of our method is the Depth-Aware Pose Motion representation (DA-PoTion), a new video descriptor that encodes the 3D movement of semantic keypoints of the human body. Given a video, we produce human joint heatmaps for each frame using a state-of-the-art 3D human pose regressor and we give each of them a unique color code according to the relative time in the clip. Then, we aggregate such 3D time-encoded heatmaps for all human joints to obtain a fixed-size descriptor (DA-PoTion), which is suitable for classifying actions using a shallow 3D convolutional neural network (CNN). The DA-PoTion alone defines a new state-of-the-art on the Penn Action Dataset. Moreover, we leverage the intrinsic complementarity of our pose motion descriptor with appearance based approaches by combining it with Inflated 3D ConvNet (I3D) to define a new state-of-the-art on the JHMDB Dataset.

1. Introduction

Recognizing actions performed by humans is an ever-green problem for the computer vision community. Action recognition involves identification of different activities from video clips. The classification of human actions presents applications in several fields, e.g. entertainment, video retrieval, and also many safety-critical tasks such as human-robot interaction and video surveillance [10, 2, 20].

Currently, most state-of-the-art methods for action recognition are 2D-based, and can rely on appearance, op-

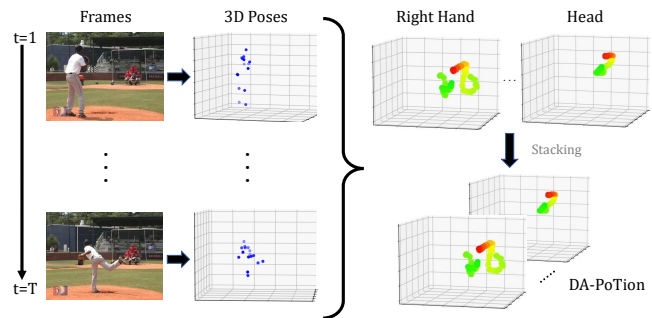


Figure 1. An example of our depth-aware PoTion representation. Given a video, it encodes the 3D movement of semantic keypoints of the human body in a volumetric descriptor.

tical flow or pose features [34, 7, 24, 36, 25]. Carreira *et al.* [7] recently proposed a two-stream CNN approach [36] that jointly considers both appearance and motion, obtaining state-of-the-art performance. Their method processes appearance information using RGB data, while motion is taken into account by leveraging optical flow images.

Furthermore, pose features have also shown to be effective in recognizing actions [9, 8, 25]. Such techniques first estimate body poses from single images or frame sequences, which are then fed as input to action recognition models. However, these methods mostly rely on 2D pose information and cannot always achieve the same robustness and accuracy as human vision. Indeed, many action recognition datasets feature both the same action appearing in several different viewpoints and different actions having the same 2D projection. Consequently, 2D pose action recognition methods are bound to fail the classification task in these situations. The Depth-Aware Pose Motion representation we propose, on the other hand, being endowed with depth-awareness, can overcome this crucial limitation and achieve high classification accuracy also for fine-grained actions.

Moreover, most of the popular techniques for action classification generally require pre-trained neural networks [7, 13, 8, 36]. In our work, we manage to overcome this limi-

tation, since our proposed video descriptor is *compact* and *fixed-size*, and we directly use it as input to train a CNN *from scratch* for action recognition.

By relying only on 3D pose features, the framework we propose is particularly suitable for solving problems that arise from cluttered scenes and variations in viewpoint, clothing and body shape. However, as can be inferred from Figure 5, a potential drawback of just considering pose features is that actions involving similar 3D movements, *e.g. tennis serve* and *baseball pitch*, can be misclassified. Nevertheless, we overcome this issue thanks to the complementarity of our framework with appearance-based models, such as the work by Carreira *et al.* [7]. In fact, by combining our DA-PoTion with their Inflated 3D Convnet architecture, we define a new state-of-the-art on the JHMDB Dataset [19].

We evaluate our method on Penn-Action [53] and JHMDB datasets [19], outperforming the baseline provided by the 2D pose motion descriptor [9] and competing with other state-of-the-art methods.

2. Related Work

2.1. Pose Estimation

While 2D pose estimation algorithms can now achieve human-like precision [27], 3D pose recovery is still an open research topic, and has gained major interest in the past few years. Furthermore, as it is difficult to build an in-the-wild dataset with ground-truth 3D annotations [44], most of the datasets are recorded in lab-like controlled environments. As a consequence, many 3D pose estimators suffer from low transferability to unseen domains.

Pavlakos *et al.* [30], on the other hand, approach the task with a unified architecture, derived from the ‘stacked hourglass network’ [28], that produces a volumetric output featuring per-voxel likelihood for each joint. Zhou *et al.* [54] developed the architecture that we use in this paper. They specifically tackle the topic of 3D pose retrieval in-the-wild, proposing a weakly-supervised transfer learning approach that uses mixed 2D and 3D labels in a unified deep-learning architecture. Their main contribution is a 3D pose regressor which can be trained end-to-end with both 2D-annotated in-the-wild images and in-the-lab images with 3D annotations.

2.2. Action Recognition

We survey four possible approaches towards action recognition. At first we examine action recognition methods not involving deep learning, and then we consider deep learning approaches leveraging respectively video features, pose features, and both video and pose features combined.

Before deep learning Early action recognition frameworks relied mainly on hand-crafted features [22], such as bag-of-words [33, 11] or action shape [4]. Such specific

features allow the direct learning of action assignments through simple classifiers, such as Support Vector Machines [33, 23, 26] or K-Nearest Neighbors [4, 43]. Wang *et al.* [45] introduced a bag-of-features descriptor consisting of ‘Histograms of Oriented Gradients’, ‘Optical Flow’ and ‘Motion Boundaries’ to represent dense trajectories, which are then classified into actions using a kernelized-SVM. Other methods handle videos as a composition of temporal segments, and train sequential state models, like Hidden Markov Models [12], Conditional Random Fields [48] and Structured SVM [29, 41] to learn the evolution of human pose and appearance throughout the video. Despite achieving promising results, all these methods rely on ad-hoc features that require intensive pre-processing and domain specific knowledge [22]. Hence, latest research works have shifted their focus towards deep learning techniques, since neural networks can extract task-dependent features autonomously and in an efficient way [51].

Video features Deep learning models that rely on video features process only appearance and motion information. Appearance data is given by the raw RGB frames, whereas motion information is obtained by computing optical flow on the video.

The ‘two-stream architecture’ is a very influential model proposed by Simonyan *et al.* [36]. The model they propose includes one spatial stream network that processes individual RGB frames and one temporal stream network which processes multiple optical flow maps. In the approach proposed by Gao *et al.* [13], a deep learning model learns to regress the optical flow map of future movements from a single RGB image. Then, the RGB frame and the learned motion map are combined as input to a classifier for action recognition. Fergus *et al.* [42], on the other hand, propose a simple approach towards spatio-temporal convolutions over a video. After learning spatio-temporal features for each video using a 3D-CNN, they use a naive linear classifier for action recognition. Finally, Carreira *et al.* [7] propose the Inflated 3D ConvNet architecture. In I3D, filters and pooling kernels of deep image classification networks are given a third dimension to learn spatio-temporal features for each video. The authors propose to train two separate I3D models, one for RGB appearance information and one for smooth optical flow maps. The resulting scores of the two networks are averaged at test time.

Pose features Another category of approaches towards action recognition consists in only considering pose features.

Iqbal *et al.* [18] propose a recursive approach for tackling both pose estimation and action recognition. Their method is twofold and iterates over a loop, since it learns to predict pose estimates from the distribution of actions

and vice versa at the same time. Finally, Choutas *et al.* [9] propose the pose motion (PoTion) descriptor, a fixed-size 2D representation that jointly encodes pose and motion of human joints. After extracting 2D pose heatmaps for all human joints in a video, they temporally aggregate them to obtain a compact descriptor that can be classified into actions using a shallow CNN.

Pose and video features The combination of pose and video features is often the method of choice for action recognition, because it allows to take the best out of the two approaches.

Liu *et al.* [24] propose two descriptors, the appearance-based Dynamic Texture Image (DTI) and the pose-based Dynamic Pose Image (DPI). The DTI is a pose-guided video frame feature obtained via an attention-based mechanism. The DPI representation is the sequence of joint estimation heatmaps. In contrast to our DA-PoTion, the DPI has many drawbacks: first, it is not fixed-size, as the length of the sequence depends on the length of the clip, second, it does not encode smooth time-encoded trajectories, and third, it does not leverage 3D pose information.

Luvizon *et al.* [25] propose a unified framework for 2D/3D pose estimation and action recognition. Features extracted from the RGB frames are firstly fused with joint heatmaps to provide appearance recognition, which is then combined with the 2D/3D estimated poses to yield the action prediction. As will be further discussed in Section 4, even though their proposed framework includes 3D pose predictions, it does not encode them into a volumetric representation as we do in the DA-PoTion. Rather, it encodes information in a sparse, scarcely-correlated manner.

The Pose-CNN descriptor proposed by [8], on the other hand, aggregates motion and appearance information along directions of human joints. The proposed model leverages pose information to guide the attention of RGB and optical flow feature extractors.

3. Method

In this Section we present our end-to-end 3D action recognition framework. Our method is divided into three stages: given a video,

- (i) we extract human joint heatmaps for each frame;
- (ii) we assign a unique color code to each joint heatmap depending on the relative time in the video clip, and we aggregate them to obtain a fixed-size descriptor, the DA-PoTion. The resulting representation gracefully fuses pose and motion information and summarizes the whole video;
- (iii) we use these descriptors to train from scratch a shallow 3D-CNN for action classification.

3.1. 3D Pose Extraction

In the first stage of our framework, we regress 3D joint positions for a single subject in the scene. To accomplish this task, we use the state-of-the-art weakly-supervised algorithm proposed by Zhou *et al.* [54], as we found it to generalize much better to in-the-wild images, if compared to other tested approaches [30, 55]. We chose not to fine-tune the pose estimator on each dataset, since we wanted our framework to be as general as possible. The algorithm takes as input a still image and a bounding-box around the human subject and returns predicted 3D positions for $J = 16$ human joints. The 2D x and y coordinates refer to the bounding-box coordinate frame, whereas the depth z coordinate refers to the absolute camera frame. Each coordinate is discretized into 256 values.

When dealing with a dataset which does not provide bounding box annotations, or with in-the-wild videos, we predict a bounding-box around the subject using YOLOv3 [31]. This is often the case for standard action recognition datasets, such as HMDB [19] or UCF-101 [37].

3.2. DA-PoTion

To represent each video, we propose a compact volumetric descriptor that embodies the 3D trajectories of human joints. Unlike the representation proposed by Choutas *et al.* [9], our descriptor for action recognition is endowed with depth-awareness. Hence, we call it Depth-Aware Pose Motion (*DA-PoTion*) representation.

In the following, we will describe the process to create the DA-PoTion *for a single human joint*. Denoting by T the number of frames in a video, we first convert the T predicted 2D coordinates (x, y) from the bounding-box coordinate frame into the coordinate frame of the original image. Such transformation is achieved by rescaling their values into the size of the original image and then summing the coordinates of the upper-left corner of the bounding-box of each frame, (x_{ul}, y_{ul}) . By doing this operation, the *DA-PoTion* can encode movements relative to all the camera frame, and its field of view is not restricted to just the motion happening inside the bounding-box. The immediate consequence of this design choice is that the *DA-PoTion* can distinguish between fine-grained actions such as running and running on the spot.

Then, for each frame, we convert the T predicted point-estimates for the 3D positions into volumetric heatmaps. This is achieved by applying to a $W \times H \times D$ volume a 3D multivariate Gaussian centered at the point-estimates, where W , H and D stand for width, height and depth respectively. We denote each of these synthetic heatmaps for a given joint j as $\mathcal{H}_j^t[x, y, z]$, for $t \in \{1, 2, \dots, T\}$.

These heatmaps, then, undergo what we call a colorization process, yielding T colored heatmaps $\mathcal{C}_j^t[x, y, z, c]$ of dimension $W \times H \times D \times C$. We colorize the heatmaps by as-

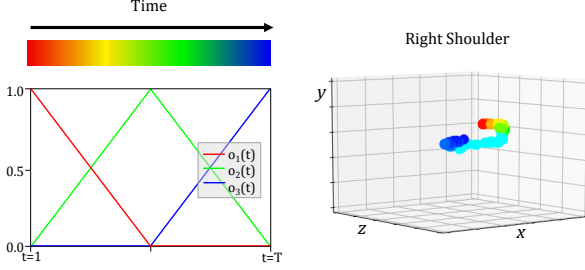


Figure 2. Illustration of the colorization scheme for $C = 3$ (left) and an example of the resulting DA-PoTion representation (right).

signing to each of the \mathcal{H}_j^t a unique code using C channels, taking inspiration from the 2D-PoTion descriptor [9]. For each t , we compute a code vector $o(t) \in \mathbb{R}^C$. For values of C up to 3, we can think $o(t)$ to represent a color vector with C channels. An example of colorization scheme is depicted in Figure 2. For $C = 2$, $o(t)$ is defined as follows:

$$o(t) = \left(\frac{t-1}{T-1}, 1 - \frac{t-1}{T-1} \right)^\top. \quad (1)$$

The extension to a generic number of channels can be done by splitting the T frames into $C - 1$ equally sampled intervals. For each of these intervals, we apply the colorization scheme with 2 channels out of C total. The final colored heatmap for frame t is given by:

$$\mathcal{C}_j^t[x, y, z, c] = \mathcal{H}_j^t[x, y, z] \cdot o_c(t). \quad (2)$$

For a given joint j , the colored heatmaps are then summed up over time, yielding a C -channel volume \mathcal{S}_j , whose size does not depend on the length of the video:

$$\mathcal{S}_j[x, y, z, c] = \sum_{t=1}^T \mathcal{C}_j^t[x, y, z, c]. \quad (3)$$

Still considering a single joint, we now propose three different aggregation schemes, yielding three different versions of the DA-PoTion.

Since the values of \mathcal{S}_j are obtained by summing over time, they depend on the number of frames. Therefore, we normalize each channel $c \in \{1, 2, \dots, C\}$ independently dividing by the maximum value over all voxels. This operation defines the first, standard aggregation scheme, which we will call *DA Unnormalized PoTion*. It is denoted by $\mathcal{U}_j[x, y, z, c]$ and it is computed as follows:

$$\mathcal{U}_j[x, y, z, c] = \frac{\mathcal{S}_j[x, y, z, c]}{\max_{x', y', z'} \mathcal{S}_j[x', y', z', c]}. \quad (4)$$

Figure 3 shows, in the top row, an example of \mathcal{U}_j at in-

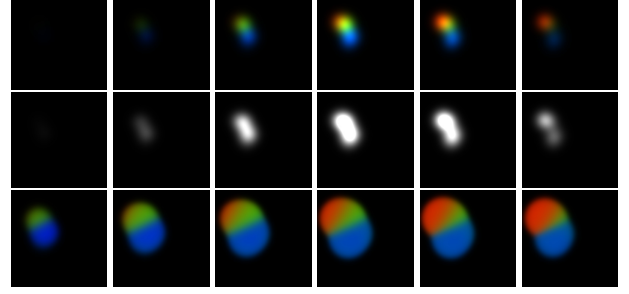


Figure 3. Examples of DA-PoTion representations for a single human joint. From left to right: increasing levels of depth. Top row: \mathcal{U}_j ; middle row: \mathcal{I}_j ; bottom row: \mathcal{N}_j .

creasing depth levels. Notice how the time information is encoded in the color of the trajectories. The second aggregation scheme yields the *DA Intensity PoTion* and it is computed as follows:

$$\mathcal{I}_j[x, y, z] = \sum_{c=1}^C \mathcal{U}_j[x, y, z, c]. \quad (5)$$

Figure 3 shows, in the middle row, an example of \mathcal{I}_j at increasing depth levels. If a joint stays at a given 3D position for a non-trivial time, then a stronger intensity will be accumulated in \mathcal{U}_j and \mathcal{I}_j . The third aggregation scheme, on the other hand, is defined in such a way to give all positions of the motion trajectory the same weight.

The third aggregation scheme yields the *DA Normalized PoTion* and it is computed as follows:

$$\mathcal{N}_j[x, y, z, c] = \frac{\mathcal{U}_j[x, y, z, c]}{\epsilon + \mathcal{I}_j[x, y, z, c]}, \quad (6)$$

with $\epsilon = 1$ to avoid instabilities in areas with low intensity. Figure 3 shows, in the bottom row, an example of \mathcal{N}_j at increasing depth levels. Notice, in contrast to the top and middle rows of the Figure, how all the steps of the trajectory are weighted equally, regardless of the time spent at each location.

This intrinsic structural difference suggests that the three aggregation schemes convey complementary information and that high classification accuracy can be achieved by stacking \mathcal{N} , \mathcal{U} and \mathcal{I} together in what will be referred to as $\mathcal{N} + \mathcal{U} + \mathcal{I}$.

The final DA-PoTion representation for a given aggregation scheme is obtained by stacking the DA-PoTion representations for all human joints.

3.3. Action Classification

Once the DA-PoTion representations for each video in the considered dataset are collected, our framework classifies these descriptors into actions. Since the DA-PoTions

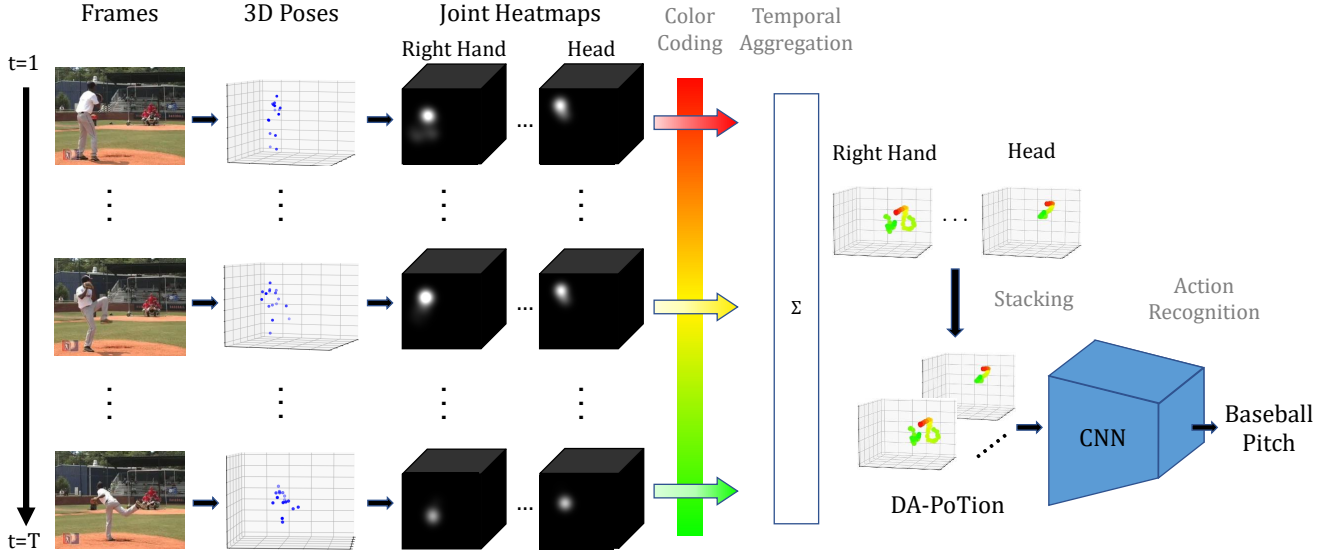


Figure 4. Illustration of our end-to-end framework for action recognition (with number of color channels $C = 2$). Given a video, (i) we produce 3D human joint heatmaps for each frame; (ii) we assign a unique code to each of them according to the relative time of the frame in the video clip; (iii) we aggregate the 3D time-encoded heatmaps for all human joints to obtain the clip-level, fixed-size DA-PoTion representation. (iv) The resulting descriptor is then fed as input into a shallow 3D-CNN trained for action classification.

are fixed-size and have significantly less texture than a normal image, we were able to classify them with just a shallow 3D-CNN without any pre-training.

Figure 4 illustrates the shallow 3D-CNN architecture that we used to classify the DA-PoTion descriptors. The input to the network for one clip is the DA-PoTion representation stacked for all human joints. When using the \mathcal{U} or the \mathcal{N} aggregation scheme, the input is composed of $J \times C$ channels, where J is the number of joints detected by the pose estimator. When using \mathcal{I} , the input is composed of just J channels and, when using the $\mathcal{N} + \mathcal{U} + \mathcal{I}$ aggregation scheme, the input is composed of $J \times (2C + 1)$ channels. Each channel is resized from $W \times H \times D$ to $64 \times 64 \times 64$. The network consists of three blocks, each composed of two 3D convolutional layers. Each convolution has a kernel size of $3 \times 3 \times 3$ and is followed by a dropout layer [38] with drop rate $p = 0.25$, batch normalization [17] and ReLU non-linearity. The first convolution in each block has a stride of 1 and the second one has a stride of 2. Therefore, the spatial resolution of each dimension is halved after each block. Finally, after the three convolutional blocks, we perform global average pooling followed by a fully-connected layer with soft-max non-linearity to perform video classification.

Training details We initialize all the layers’ weights using Xavier initialization [16]. Then we optimize the network parameters over 100 epochs using Adam [21] optimizer, with an exponentially decaying learning rate. It

took approximately 2 days to train our 3D-CNN on a single GPU NVIDIA GeForce GTX 1060.

During training, we use *data augmentation* to improve generalization. Each input sample first goes through a random affine transformation, yielding a translated and rotated output, which is then randomly flipped about the y and z axes.

3.4. Fusing the DA-PoTion with I3D

Since our framework only relies on pose information, its predictions are complementary to the ones produced by I3D [7] and other approaches that process video features (RGB and optical flow). For this reason, we implemented in our framework the possibility to fuse the predictions made by the two models.

At training time, the two models are trained separately, with the DA-PoTion following the approach described in Sections 3.1, 3.2 and 3.3, and the I3D model following the procedure reported in [7]. At test time, each video is fed into the DA-PoTion framework, the RGB I3D network and the optical flow I3D network, producing three sets of per-action scores. We then obtain the final score for each action by averaging the three scores with equal weights.

4. Results

We ran extensive experiments to validate our approach. Table 1 reports our performance against the 2D PoTion [9] baseline, Tables 3, 4, and 2 present the results of our ablation study and Table 5 presents the comparison of our results

Method	Ground-truth	Penn Action
2D PoTion [9]	-	93.6
2D PoTion [9]	✓	95.6
DA-PoTion	-	96.3

Table 1. Classification accuracy on the Penn Action Dataset. All experiments were run with $C = 3$ channels and $\mathcal{N} + \mathcal{U} + \mathcal{I}$ aggregation scheme. ‘Ground-truth’ denotes that ground-truth pose annotations were used to compute the result.

Method	σ	Penn Action
DA-PoTion	$2\sqrt{2}$	93.6
DA-PoTion	4	96.3
DA-PoTion	$4\sqrt{2}$	51.7

Table 2. Classification accuracy on Penn Action Dataset when varying standard deviation σ of the Gaussian mask applied on the pose point-predictions. The experiments were run with $C = 3$ channels and aggregation scheme $\mathcal{N} + \mathcal{U} + \mathcal{I}$.

Method	Channels	Penn Action
2D PoTion [9]	2	90.8
2D PoTion [9]	3	93.6
2D PoTion [9]	4	94.2
DA-PoTion	2	94.1
DA-PoTion	3	96.3
DA-PoTion	4	97.2

Table 3. Classification accuracy on the Penn Action Dataset when varying the number of channels C . The experiments were run with $\sigma = 4$ and aggregation scheme $\mathcal{N} + \mathcal{U} + \mathcal{I}$.

with the state-of-the-art. We tested our end-to-end framework on the *Penn Action* [53] and *JHMDB* [19] datasets. Our results are reported as mean classification accuracy.

The Penn Action Dataset contains 2326 videos from 15 classes. It features a single subject per video and it is annotated with action, 2D ground-truth joint positions, and bounding-boxes around the subject. The JHMDB Dataset contains 928 videos from 21 classes. It can feature multiple subjects in the scene. All videos are annotated with 2D ground-truth joint positions for only one subject. The *sub-JHMDB* Dataset is a subset of JHMDB containing only 12 actions.

Baseline comparison As a first experiment, we wanted to compare our performance to the 2D PoTion approach by Choutas *et al.* [9], the baseline to our work. Table 1 presents our result on the Penn Action Dataset and compares it with the classification accuracy achieved by 2D PoTion. In order to assess an upper bound for the performance of the 2D PoTion architecture, we ran their framework using the ground-truth annotations of the 2D poses, instead of predicting them. As we perform better than the 2D PoTion also in this extreme case, we can safely claim that our approach outperforms the baseline.

Method	Type	Penn Action
2D PoTion [9]	\mathcal{U}	89.7
2D PoTion [9]	$\mathcal{N} + \mathcal{U} + \mathcal{I}$	93.6
DA-PoTion	\mathcal{U}	95.9
DA-PoTion	$\mathcal{N} + \mathcal{U} + \mathcal{I}$	96.3

Table 4. Classification accuracy on the Penn Action Dataset when varying the aggregation scheme. The experiments were run with $\sigma = 4$ and $C = 3$ channels.

	Method	Accuracy		
		sub-JHMDB	JHMDB	Penn Action
Video features	Im2Flow [13]	-	-	77.4
	DT [45]	46.0	-	73.4
	C3D [42]	68.8	-	86.0
	I3D [7]	-	84.1	-
Pose features	HLPF [19]	51.1	-	-
	ACPS [18]	61.5	-	79.0
	2D PoTion [9]	-	57.0	93.6
	DA-PoTion (Ours)	71.5	70.4	97.2
Pose+ Video features	IDT-FV [46]	60.9	-	92.0
	DTI+DPI [24]	-	-	95.86
	Luvizon <i>et al.</i> [25]	-	-	97.4*
	MST-AOG [47]	45.3	-	74.0
	ST-AOG [49]	61.2	-	85.5
	P-CNN [8]	66.8	61.1	95.3
	Action Tubes [15]	-	62.5	-
	ACPS+IDT-FV [18]	74.6	-	92.9
	JDD [5]	79.7	-	95.3
	Zolfaghari <i>et al.</i> [56]	-	76.1	-
	2D PoTion + I3D [9]	-	85.5	-
DA-PoTion (Ours) + I3D	-	87.8	-	

Table 5. Comparison between our method and the state-of-the-art on the Penn Action, JHMDB and subJHMDB datasets. ‘Video features’ refer to methods using appearance and motion information; ‘pose features’ refer to methods using only pose features. The asterisk denotes that fine-tuning was performed on the pose estimator for the specific dataset. In bold the best method; underlined the best method among those that leverage only pose features.

Ablation study In Table 2 we explore the effect of changing the variance of the Gaussian mask that is applied to the joint point-predictions extracted by the 3D pose regressor. In Tables 3 and 4, on the other hand, we study the impact of varying number of channels and aggregation schemes in both the 2D PoTion and in our DA-PoTion representation.

In Table 2 we highlight the importance of choosing the appropriate variance when creating Gaussian heatmaps from pose point-predictions. Empirically, we find out that using a variance of 16 pixels, that is a standard deviation of 4 pixels, represents the best trade-off between smoothness and sparsity of the representation. Indeed, when using a smaller variance, the resulting DA-PoTion suffers from noise and discretization errors, and hence it cannot encode smooth, continuous movements of the joints. This results in a slight degradation of the classification accuracy, as re-

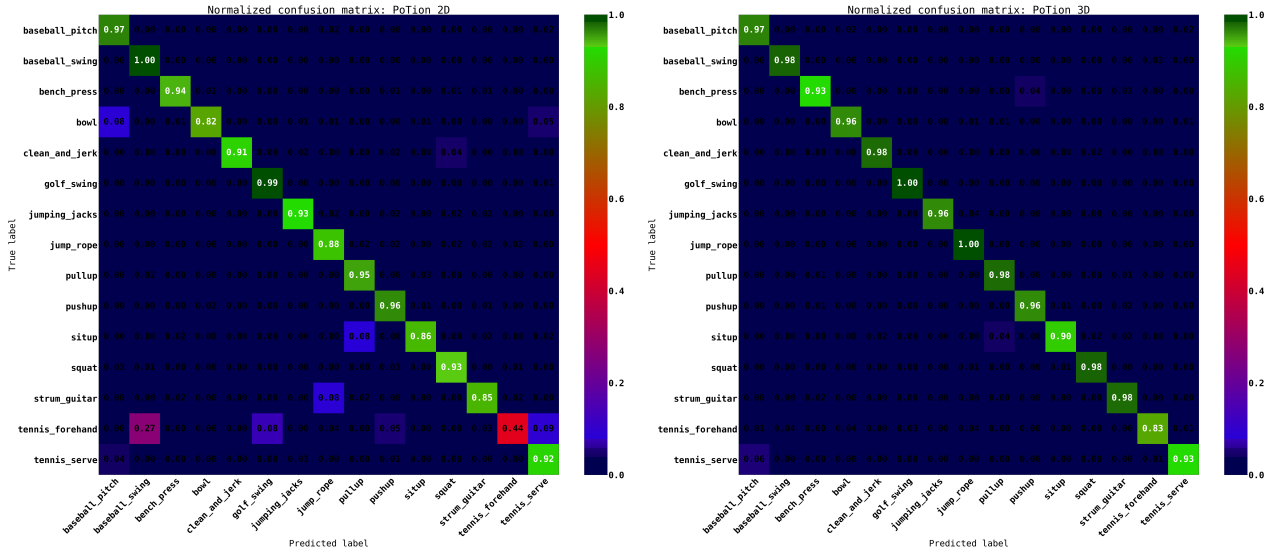


Figure 5. Confusion matrices for action classification on the Penn Action Dataset. Left: 2D PoTion; right: DA-PoTion.

ported in the first row of Table 2. On the other hand, as the last row of Table 2 testifies, when using a bigger variance, the resulting DA-PoTion is almost not informative at all. In fact, having such a large variance causes the joint trajectories time-encoded in the DA-PoTion to have a thickness that covers almost all the volume of the representation. Clearly, in such a scenario the 3D-CNN used for action classification cannot distinguish neither coarse-grained nor fine-grained movements.

In Table 3, we observe a clear improvement for both the 2D PoTion and DA-PoTion when increasing the number of channels from 2 to 4. Nevertheless, a 4-channel DA-PoTion resulted very computationally expensive. For this reason, for all subsequent results, we report results with $C = 3$ as a trade-off between accuracy and compactness of the representation.

In Table 4, we observe that the $\mathcal{N} + \mathcal{U} + \mathcal{I}$ aggregation scheme outperforms the *Unnormalized PoTion* \mathcal{U} for the 2D case by a greater mean than for our method. Note that the likelihood of having a joint staying at the same 3D position for a non-trivial time, which would lead to differences between \mathcal{N} , \mathcal{U} and \mathcal{I} , is much lower than the likelihood of the same event happening in the 2D setting. For the 2D PoTion, stacking the three aggregation schemes conveys additional information that is very useful to distinguish fine-grained actions. This additional information is already intrinsic in our depth-aware representation, even for \mathcal{U} .

Comparison to state-of-the-art In Table 5, we provide a detailed comparison between our method and

other state-of-the-art approaches on the Penn Action, JHMDB, sub-JHMDB datasets. We can observe that our framework reaches state-of-the-art accuracy on all three datasets among the methods that only consider pose features. Moreover, we define a new state-of-the-art on the Penn Action Dataset [53]. The only result that competes with ours, [25], is obtained by fine-tuning its embedded pose regressor on this specific dataset, which we chose not to do in order to improve generalization.

Combining our approach with I3D [7] in the way described in Section 3.4, we also define a new state-of-the-art on the JHMDB Dataset [19].

Penn Action Dataset performance analysis As can be seen from the confusion matrices in Figure 5, we consistently outperform the 2D PoTion [9] approach (left image) in all the classes. As an example, because of its lack of depth information, 2D PoTion mainly misclassifies *tennis forehand* with *baseball swing* and *golf swing*, which have similar projections on the 2D plane. Our approach (right image) is able to make the correct prediction also in this situation by leveraging 3D pose information.

Qualitative analysis of the 3D pose estimator It is worth noticing that, despite we are already using a state-of-the-art 3D pose regressor, the potential of our framework can increase even more as 3D pose regressors keep improving. In fact, Table 4 points out that, when considering ground-truth 2D pose annotations, classification accuracy grows for the 2D setting. This proves that our



Figure 6. Qualitative performance of the 3D pose estimator by Zhou *et al.* [54] on two in-the-wild images. Top: coherent 3D pose predictions; bottom: wrong 3D pose predictions.

framework could benefit all the more from improvements of 3D pose regressors. Indeed, 3D state-of-the-art pose estimators currently perform poorly compared to the 2D ones because of their scarce transferability on domains different than the training one [27]. Low transferability can also be inferred from Figure 6, where we present the qualitative performance of [54] on two in-the-wild images. As the subjects in both images are well included in the frame and well-distinguishable from the background, the main reason for the performance degradation is to be found in the domain shift from the tennis match to the ski race.

5. Conclusion

We propose an end-to-end framework for action recognition that reaches state-of-the-art performance, among the methods that rely only on pose features, on the most popular datasets for action classification. The use of our DA-PoTion representation alone already defines a new state-of-the-art on the Penn Action Dataset [53]. Since sport actions often present repetitive patterns for joint movements, which is exactly the key information encoded in our descriptor, we obtain remarkable results on this dataset featuring many sport

activities. Moreover, the combination of our pose feature with the RGB and optical flow streams of I3D [7] achieves the new state-of-the-art on the JHMDB dataset [19], proving how the complementarity of pose and video features can be beneficial to action recognition techniques. In contrast to the work of Luvizon *et al.* [25], which also uses 3D poses for action recognition, our DA-PoTion representation is an image-like 3D heatmap whose adjacent points are highly correlated and, thus, suggests the use of a 3D-CNN to learn action assignments from such a dense representation. Our approach neatly embodies strongly correlated features in a compact descriptor, whereas Luvizon *et al.* propose the use of a sparse 3D representation with scarcely correlated adjacent points. Since their descriptor presents high correlation only on the temporal axis, they are forced to use a 2D-CNN.

Additionally, being succinct and dense with information, our DA-PoTion is ideal for tasks where the simplicity of input features is crucial. For instance, action recognition frameworks that can only rely on optical-flow features, such as the work by Gao *et al.* [13], are more likely to fail than our approach, due to an excess of information in the input which is not related to the action itself. In our work, we showed how the combination of classifiers relying on inputs with different context and meaning can significantly boost the accuracy, compensating for actions for which a method is less suitable and performs poorly.

6. Future Work

The versatility and modularity of our approach allows it to be used for multiple purposes. As we employed our DA-PoTion on human joints for the task of full-body action recognition, it would be easy to adapt our framework on human hands to recognize fine-grained actions like playing piano, grasping objects, or pouring milk [50, 35, 14, 1]. Analogously, it might be interesting to further tune our approach for facial expression recognition. It would be as simple as replacing the 3D full-body pose regressor with a human face keypoint tracker [40, 3, 52].

Furthermore, given the DA-PoTion resulting from one section of a videoclip, one could train a Recurrent Neural Network (RNN) model to recursively predict future poses of the subject in the scene.

Despite our framework could easily be applied to multiple subjects simultaneously, current state-of-the-art 3D human pose predictors process only one subject at a time [54, 30, 32, 39]. Our work will therefore greatly benefit, in terms of general applicability, from advancements of 3D human pose regressors in that direction, just like the algorithm developed by Cao *et al.* [6] did for the 2D setting.

References

- [1] N. Agarwal, A. Krohn-Grimberghe, and R. Vyas. Facial key points detection using deep convolutional neural network-naimishnet. *arXiv preprint arXiv:1710.00977*, 2017. 8
- [2] S. C. Akkaladevi and C. Heindl. Action recognition for human robot interaction in industrial applications. *2015 IEEE International Conference on Computer Graphics, Vision and Information Security (CGVIS)*, pages 94–99, 2015. 1
- [3] S. Berretti, B. B. Amor, M. Daoudi, and A. Del Bimbo. 3d facial expression recognition using sift descriptors of automatically detected keypoints. *The Visual Computer*, 27(11):1021, 2011. 8
- [4] M. Blank, L. Gorelick, E. Shechtman, M. Irani, and R. Basri. Actions as space-time shapes. In *Tenth IEEE International Conference on Computer Vision (ICCV'05) Volume 1*, volume 2, pages 1395–1402. IEEE, 2005. 2
- [5] C. Cao, Y. Zhang, C. Zhang, and H. Lu. Body joint guided 3-d deep convolutional descriptors for action recognition. *IEEE transactions on cybernetics*, pages 1095–1108, 2017. 6
- [6] Z. Cao, T. Simon, S.-E. Wei, and Y. Sheikh. Realtime multi-person 2d pose estimation using part affinity fields. In *Proceedings of the IEEE Conference on Computer Vision and Pattern Recognition*, pages 7291–7299, 2017. 8
- [7] J. Carreira and A. Zisserman. Quo vadis, action recognition? a new model and the kinetics dataset. In *proceedings of the IEEE Conference on Computer Vision and Pattern Recognition*, pages 6299–6308, 2017. 1, 2, 5, 6, 7, 8
- [8] G. Cheron, I. Laptev, and C. Schmid. P-cnn: Pose-based cnn features for action recognition. In *The IEEE International Conference on Computer Vision (ICCV)*, December 2015. 1, 3, 6
- [9] V. Choutas, P. Weinzaepfel, J. Revaud, and C. Schmid. Potion: Pose motion representation for action recognition. In *CVPR 2018 - IEEE Conference on Computer Vision and Pattern Recognition*, pages 7024–7033. IEEE, 2018. 1, 2, 3, 4, 5, 6, 7
- [10] A. Ciptadi, M. S. Goodwin, and J. M. Rehg. Movement pattern histogram for action recognition and retrieval. In *European conference on computer vision*, pages 695–710. Springer, 2014. 1
- [11] P. Dollár, V. Rabaud, G. Cottrell, and S. Belongie. Behavior recognition via sparse spatio-temporal features. VS-PETS Beijing, China, 2005. 2
- [12] T. V. Duong, H. H. Bui, D. Q. Phung, and S. Venkatesh. Activity recognition and abnormality detection with the switching hidden semi-markov model. In *2005 IEEE Computer Society Conference on Computer Vision and Pattern Recognition (CVPR'05)*, volume 1, pages 838–845. IEEE, 2005. 2
- [13] R. Gao, B. Xiong, and K. Grauman. Im2flow: Motion hallucination from static images for action recognition. In *Proceedings of the IEEE Conference on Computer Vision and Pattern Recognition*, pages 5937–5947, 2018. 1, 2, 6, 8
- [14] S. Gattupalli, A. R. Babu, J. R. Brady, F. Makedon, and V. Athitsos. Towards deep learning based hand keypoints detection for rapid sequential movements from rgb images. In *Proceedings of the 11th Pervasive Technologies Related to Assistive Environments Conference*, pages 31–37. ACM, 2018. 8
- [15] G. Gkioxari and J. Malik. Finding action tubes. In *Proceedings of the IEEE conference on computer vision and pattern recognition*, pages 759–768, 2015. 6
- [16] X. Glorot and Y. Bengio. Understanding the difficulty of training deep feedforward neural networks. In *Proceedings of the thirteenth international conference on artificial intelligence and statistics*, pages 249–256, 2010. 5
- [17] S. Ioffe and C. Szegedy. Batch normalization: Accelerating deep network training by reducing internal covariate shift. *arXiv preprint arXiv:1502.03167*, 2015. 5
- [18] U. Iqbal, M. Garbade, and J. Gall. Pose for action-action for pose. In *2017 12th IEEE International Conference on Automatic Face & Gesture Recognition (FG 2017)*, pages 438–445. IEEE, 2017. 2, 6
- [19] H. Jhuang, J. Gall, S. Zuffi, C. Schmid, and M. J. Black. Towards understanding action recognition. In *The IEEE International Conference on Computer Vision (ICCV)*, December 2013. 2, 3, 6, 7, 8
- [20] S. Ji, W. Xu, M. Yang, and K. Yu. 3d convolutional neural networks for human action recognition. *IEEE transactions on pattern analysis and machine intelligence*, 35(1):221–231, 2012. 1
- [21] D. P. Kingma and J. Ba. Adam: A method for stochastic optimization. *arXiv preprint arXiv:1412.6980*, 2014. 5
- [22] Y. Kong and Y. Fu. Human action recognition and prediction: A survey. *CoRR*, abs/1806.11230, 2018. 2
- [23] I. Laptev, M. Marszałek, C. Schmid, and B. Rozenfeld. Learning realistic human actions from movies. 2008. 2
- [24] M. Liu, F. Meng, C. Chen, and S. Wu. Joint dynamic pose image and space time reversal for human action recognition from videos. 2019. 1, 3, 6
- [25] D. C. Luvizon, D. Picard, and H. Tabia. 2d/3d pose estimation and action recognition using multitask deep learning. In *The IEEE Conference on Computer Vision and Pattern Recognition (CVPR)*, June 2018. 1, 3, 6, 7, 8
- [26] M. Marszałek, I. Laptev, and C. Schmid. Actions in context. In *CVPR 2009-IEEE Conference on Computer Vision & Pattern Recognition*, pages 2929–2936. IEEE Computer Society, 2009. 2
- [27] A. Martínez-González, M. Villamizar, O. Canévet, and J.-M. Odobez. Investigating depth domain adaptation for efficient human pose estimation. In *Proceedings of the European Conference on Computer Vision (ECCV)*, pages 0–0, 2018. 2, 8
- [28] A. Newell, K. Yang, and J. Deng. Stacked hourglass networks for human pose estimation. In *European Conference on Computer Vision*, pages 483–499. Springer, 2016. 2
- [29] J. C. Niebles, C.-W. Chen, and L. Fei-Fei. Modeling temporal structure of decomposable motion segments for activity classification. In *European conference on computer vision*, pages 392–405. Springer, 2010. 2
- [30] G. Pavlakos, X. Zhou, K. G. Derpanis, and K. Daniilidis. Coarse-to-fine volumetric prediction for single-image 3d human pose. In *Proceedings of the IEEE Conference on Com-*

- puter Vision and Pattern Recognition, pages 7025–7034, 2017. 2, 3, 8
- [31] J. Redmon and A. Farhadi. Yolov3: An incremental improvement. *arXiv preprint arXiv:1804.02767*, 2018. 3
- [32] H. Rhodin, M. Salzmann, and P. Fua. Unsupervised geometry-aware representation for 3d human pose estimation. In *Proceedings of the European Conference on Computer Vision (ECCV)*, pages 750–767, 2018. 8
- [33] C. Schuldt, I. Laptev, and B. Caputo. Recognizing human actions: a local svm approach. In *Proceedings of the 17th International Conference on Pattern Recognition, 2004. ICPR 2004.*, volume 3, pages 32–36. IEEE, 2004. 2
- [34] L. Sevilla-Lara, Y. Liao, F. Güney, V. Jampani, A. Geiger, and M. J. Black. On the integration of optical flow and action recognition. In *German Conference on Pattern Recognition*, pages 281–297. Springer, 2018. 1
- [35] T. Simon, H. Joo, I. Matthews, and Y. Sheikh. Hand keypoint detection in single images using multiview bootstrapping. In *Proceedings of the IEEE conference on Computer Vision and Pattern Recognition*, pages 1145–1153, 2017. 8
- [36] K. Simonyan and A. Zisserman. Two-stream convolutional networks for action recognition in videos. In *Advances in neural information processing systems*, pages 568–576, 2014. 1, 2
- [37] K. Soomro, A. R. Zamir, and M. Shah. Ucf101: A dataset of 101 human actions classes from videos in the wild. *arXiv preprint arXiv:1212.0402*, 2012. 3
- [38] N. Srivastava, G. Hinton, A. Krizhevsky, I. Sutskever, and R. Salakhutdinov. Dropout: a simple way to prevent neural networks from overfitting. *The Journal of Machine Learning Research*, 15:1929–1958, 2014. 5
- [39] X. Sun, B. Xiao, F. Wei, S. Liang, and Y. Wei. Integral human pose regression. In *Proceedings of the European Conference on Computer Vision (ECCV)*, pages 529–545, 2018. 8
- [40] Y. Sun, X. Wang, and X. Tang. Deep convolutional network cascade for facial point detection. In *The IEEE Conference on Computer Vision and Pattern Recognition (CVPR)*, June 2013. 8
- [41] K. Tang, L. Fei-Fei, and D. Koller. Learning latent temporal structure for complex event detection. In *2012 IEEE Conference on Computer Vision and Pattern Recognition*, pages 1250–1257. IEEE, 2012. 2
- [42] D. Tran, L. Bourdev, R. Fergus, L. Torresani, and M. Paluri. Learning spatiotemporal features with 3d convolutional networks. In *Proceedings of the IEEE international conference on computer vision*, pages 4489–4497, 2015. 2, 6
- [43] D. Tran and A. Sorokin. Human activity recognition with metric learning. In *European conference on computer vision*, pages 548–561. Springer, 2008. 2
- [44] T. von Marcard, R. Henschel, M. J. Black, B. Rosenhahn, and G. Pons-Moll. Recovering accurate 3d human pose in the wild using imus and a moving camera. In *Proceedings of the European Conference on Computer Vision (ECCV)*, pages 601–617, 2018. 2
- [45] H. Wang, A. Kläser, C. Schmid, and C.-L. Liu. Dense trajectories and motion boundary descriptors for action recognition. *International journal of computer vision*, 103(1):60–79, 2013. 2, 6
- [46] H. Wang and C. Schmid. Action recognition with improved trajectories. In *Proceedings of the IEEE international conference on computer vision*, pages 3551–3558, 2013. 6
- [47] J. Wang, X. Nie, Y. Xia, Y. Wu, and S.-C. Zhu. Cross-view action modeling, learning and recognition. In *Proceedings of the IEEE Conference on Computer Vision and Pattern Recognition*, pages 2649–2656, 2014. 6
- [48] S. B. Wang, A. Quattoni, L.-P. Morency, D. Demirdjian, and T. Darrell. Hidden conditional random fields for gesture recognition. In *2006 IEEE Computer Society Conference on Computer Vision and Pattern Recognition (CVPR'06)*, volume 2, pages 1521–1527. IEEE, 2006. 2
- [49] B. Xiaohan Nie, C. Xiong, and S.-C. Zhu. Joint action recognition and pose estimation from video. In *Proceedings of the IEEE Conference on Computer Vision and Pattern Recognition*, pages 1293–1301, 2015. 6
- [50] S. Yuan, G. Garcia-Hernando, B. Stenger, G. Moon, J. Yong Chang, K. Mu Lee, P. Molchanov, J. Kautz, S. Honari, L. Ge, et al. Depth-based 3d hand pose estimation: From current achievements to future goals. In *Proceedings of the IEEE Conference on Computer Vision and Pattern Recognition*, pages 2636–2645, 2018. 8
- [51] M. D. Zeiler and R. Fergus. Visualizing and understanding convolutional networks. In *European conference on computer vision*, pages 818–833. Springer, 2014. 2
- [52] S. Zhang and C. Meng. Facial keypoints detection using neural network. *Stanford Report*, 2016. 8
- [53] W. Zhang, M. Zhu, and K. G. Derpanis. From actemes to action: A strongly-supervised representation for detailed action understanding. In *Proceedings of the IEEE International Conference on Computer Vision*, pages 2248–2255, 2013. 2, 6, 7, 8
- [54] X. Zhou, Q. Huang, X. Sun, X. Xue, and Y. Wei. Towards 3d human pose estimation in the wild: a weakly-supervised approach. In *Proceedings of the IEEE International Conference on Computer Vision*, pages 398–407, 2017. 2, 3, 8
- [55] X. Zhou, A. Karpur, L. Luo, and Q. Huang. Starmap for category-agnostic keypoint and viewpoint estimation. *CoRR*, abs/1803.09331, 2018. 3
- [56] M. Zolfaghari, G. L. Oliveira, N. Sedaghat, and T. Brox. Chained multi-stream networks exploiting pose, motion, and appearance for action classification and detection. In *The IEEE International Conference on Computer Vision (ICCV)*, 2017. 6